V International Conference on Particle-based Methods – Fundamentals and Applications
PARTICLES 2017
P. Wriggers, M. Bischoff, E. Oñate, D.R.J. Owen, & T. Zohdi (Eds)

HYDRO-MECHANICAL COUPLED DUAL DOMAIN MATERIAL POINT METHOD STABILIZED WITH A NULL-SPACE FILTER

Q. A. TRAN[1], W.T. SOŁOWSKI[2] AND E. CUMMINGS[3]

[1] Department of Civil Engineering, Aalto University
Rakentajanaukio 4 A, 02150 Espoo, Finland
tran.quocanh@aalto.fi

[2] Department of Civil Engineering, Aalto University
Rakentajanaukio 4 A, 02150 Espoo, Finland
wojciech.solowski@aalto.fi

[3] Department of Civil Engineering, Aalto University
Rakentajanaukio 4 A, 02150 Espoo, Finland
evan.cummings@aalto.fi

Key words: Large strain modelling, hydro-mechanical coupling, Material Point Method, Dual Domain Material Point Method, null-space filter.

Abstract. The Material Point Method (MPM) is a continuum-based numerical method especially suitable for solving large deformation problems. In this paper, we investigate the null-space errors present in MPM solutions. The paper establishes a null-space stability condition which is used to examine the null-space errors in different versions of the MPM. This analysis shows that a B-splines MPM satisfies the null-space stability condition and therefore reduces greatly the errors associated with the null-space. In contrast, the MPM, the Generalized Interpolation Material Point Method (GIMP) and the Dual Domain Material Point Method (DDMP) show non-trivial null-spaces in the mapping. To remove the null-space errors, this paper utilizes QR factorization method, which is similar to the Single Value Decomposition (SVD) method, but requires fewer computations. This paper simulates several problems with hydro-mechanical coupled Dual Domain Material Point Method (DDMP) formulation both with and without null-space error reduction. The simulations indicate that the null-space filter can improve significantly the accuracy of the pore water pressure for both gravity loading and consolidation in large strain simulation.

1. INTRODUCTION

Ringing instability problems have been defined by Brackbill [1] as a source of errors in the Particle-in-cell (PIC) method. The instability induced a large amplitude fluctuation of the

particle density in PIC caused by the mismatch of degree of freedoms between particles and grid. Edwards and Bridson [2] showed that this noise is unavoidable in PIC because of the greater number of particles than grid points. Subsequently, Gritton and Berzin [3] showed that there is a link between the ringing instability and the null-space mapping in the particle methods and adopted a Single Value Decomposition (SVD) to remove the null-space errors. Similarly, Hammerquist and Nairn [4] also proposed XPIC(m) to reduce the null-space errors from the mapping matrix.

The Material Point Method (MPM) has been based on the Particle-in-cell method [5]. Unfortunately, the Material Point Method due to similar characteristic to PIC has similar issues related to the null-space errors. This paper investigates the null-space errors in the MPM framework. It also explains why the null-space errors can be reduced when a high order of interpolation is used or there is no null-space error for the case of 1 material point per cell.

Shown results match convergence analyses of Bardenhagen and Kober [6] who proposed the Generalized Interpolation Material Point Method (GIMP). They also suggested that one material point per cell may be the optimal discretization scheme for the GIMP to minimize the errors although they could not decouple the cell-crossing errors and the ringing instability errors in the analyses. However, Tran et al. [7] showed that too few material points per cell may generate errors in the MPM when applied to gas dynamic. Therefore, reducing the number of material points per cell is not always feasible and removing the null-space errors in other way is critical. To achieve this goal, this paper develops the QR factorization method to remove the null-space to achieve the higher accuracy in the MPM formulations.

To demonstrate the capability of the QR factorization method to remove the null-space filter, this work applies the method to the hydro-mechanical coupled Dual Domain Material Point Method (DDMP) formulation [8]. While the previous versions of hydro-coupled MPM are validated successfully in the small strain benchmarks, the large strain benchmarks have not been too successful as the null space errors accumulate in-line with strains. The paper shows that by using a null-space filter, the pore water pressure can achieve a desirable accuracy for the large strain benchmark simulations. Shown benchmarks include gravity loading and large strain consolidation problems.

2. PROBLEM DEFINITION

The MPM formulations [5] has been enhanced leading, among others, to GIMP [6], [9], B-splines MPM [10] and DDMP [11]. This study utilises the stress mapping scheme in the MPM formulations as shown in Figure 1. The stress states associated with the material points and the current time step "k" ($\sigma_{\boldsymbol{p}}^{\boldsymbol{k}}$) are interpolated to the nodes, leading to the nodal internal forces ($\boldsymbol{f}_{\boldsymbol{n}}^{\boldsymbol{int,k}}$). This interpolation uses the gradient of the shape function ($\nabla\mathbf{N}$). At the nodes, the balance equations are solved to obtain the nodal velocities at the end of the time step, denoted by "L" ($\mathbf{v}_{\boldsymbol{n}}^{\boldsymbol{L}}$). Subsequently, the nodal velocity is mapped back to the gradient velocity of the material points ($\nabla\mathbf{v}_{\boldsymbol{p}}^{\boldsymbol{k+1}}$) and the compatibility and constitutive equations are used to determine the stress of material points in the next time step "k+1" ($\sigma_{\boldsymbol{p}}^{\boldsymbol{k+1}}$).

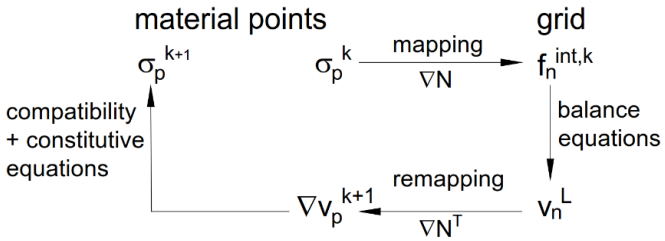

Figure 1. Schematic of stress mapping scheme in MPM

Consider a domain Ω discretised into N_p material points on a background grid with N_n nodes. The linear mapping of stress can be written in the matrix form as follows:

$$\mathbf{f}^{\mathbf{int}}_{\boldsymbol{n},\mathrm{N_n\ x\ 1}} = \nabla\mathbf{N}_{\mathrm{N_n\ x\ N_p}} \cdot \boldsymbol{\sigma}_{\boldsymbol{p},\mathrm{N_p\ x\ 1}} \tag{1}$$

where $\mathbf{f}^{\mathrm{int}}_{\boldsymbol{n},\mathrm{N_n\ x\ 1}}$ is the global nodal internal forces vector, $\boldsymbol{\sigma}_{\boldsymbol{p},\mathrm{N_p\ x\ 1}}$ is the global vector containing stress in the material points and $\nabla\mathbf{N}_{\mathrm{N_n\ x\ N_p}}$ is the linear mapping matrix, denoted as $\nabla\mathbf{N}$. Similarly, the mapping of the velocity can be written as:

$$\nabla\mathbf{v}_{\mathbf{p},\mathrm{N_p\ x\ 1}} = \nabla\mathbf{N}_{\mathrm{N_p\ x\ N_n}} \cdot \mathbf{v}^{\mathrm{L}}_{\mathbf{n},\mathrm{N_n\ x\ 1}} \tag{2}$$

where $\nabla\mathbf{v}_{\mathbf{p},\mathrm{N_p\ x\ 1}}$ is the global gradient velocity vector for all material points, $\mathbf{v}^{\mathrm{L}}_{\mathbf{n},\mathrm{N_n\ x\ 1}}$ is the global nodal velocity vector at the end of time step and $\nabla\mathbf{N}_{\mathrm{N_p\ x\ N_n}} = \nabla\mathbf{N}^{\boldsymbol{T}}_{\mathrm{N}_n\ \mathrm{x\ N}_p}$ is the linear transformation matrix, denoted $\nabla\mathbf{N}^{\mathbf{T}}$.

In the linear algebra, the rank of the linear mapping, rank($\nabla\mathbf{N}$), is defined as the number of independent vector spaces (dimensions) generated by the columns of the matrix. The null-space between two vector spaces $\mathbf{f}^{\mathrm{int}}_{\boldsymbol{n}}$ and $\boldsymbol{\sigma}_{\boldsymbol{p}}$ is the set of all elements $\boldsymbol{\sigma}^{\mathbf{null}}_{\boldsymbol{p}}$ such that $\nabla\mathbf{N}.\boldsymbol{\sigma}^{\mathbf{null}}_{\boldsymbol{p}} = 0$. The nullity of the matrix, denoted null($\nabla\mathbf{N}$) is the number of independent null-spaces generated by the columns of the matrix. According to the dimension theorem, the sum of rank and nullity is equal to either the number of columns or the number of nodes as:

$$\mathrm{rank}(\nabla\mathbf{N}) + \mathrm{null}(\nabla\mathbf{N}) = N_p \tag{3}$$

$$\mathrm{rank}(\nabla\mathbf{N}) + \mathrm{null}(\nabla\mathbf{N}^{\mathbf{T}}) = N_n \tag{4}$$

The presence of the null-space in the linear transformation leads to the instability of the solutions because the null-space can result in either no solution or infinite solutions for the eq.(1) and eq.(2). To derive an unique solution, it is necessary to produce a MPM formulation which the nullity of the transformation in eq.(3) and eq.(4) is zero. In other words, the MPM formulation can be more stable if the linear mapping ∇N is full rank (the linear mapping achieves maximum rank with $\mathrm{rank}(\nabla\mathbf{N}) = \min(N_p, N_n)$). In contrast, if ∇N is rank deficient ($\mathrm{rank}(\nabla\mathbf{N}) < \min(N_p, N_n)$), the MPM formulation may become unstable due to null-space errors. Therefore, the null-space stability condition for the MPM formulation is:

$$\begin{cases} \text{stable formulation} & \text{if } \mathrm{null}(\nabla\mathbf{N}) \text{ or } \mathrm{null}(\nabla\mathbf{N}^{\mathbf{T}}) = 0 \\ \text{unstable formulation} & \text{if } \mathrm{null}(\nabla\mathbf{N}) \text{ and } \mathrm{null}(\nabla\mathbf{N}^{\mathbf{T}}) > 0 \end{cases} \tag{5}$$

In the classical MPM, there is a non-trivial null-space in the linear mapping $\nabla\mathbf{N}$. The null-

space may induce errors in stress. However, the material point discretization affects the null-space errors. For example, one material point per cell can remove the null-space error because, in MPM, rank($\nabla\mathbf{N}$) is equal to the number of the cell. Therefore, the null-space stability condition is satisfied (rank($\nabla\mathbf{N}$) $= N_{cell} = N_p$ therefore null($\nabla\mathbf{N}$) $= 0$ in eq.(3)). However, in general, the number of material points are greater than the number of nodes ($N_p > N_n$). In these cases, the MPM formulation is susceptible to the null-space errors. Therefore, it is necessary to enhance the method with some algorithms which would lead to satisfying the null-space stability condition (5) or removing the null space errors. In the next sections, three such algorithms are presented in detail including:

- algorithm 1 –improvements in the gradient of the shape function
- algorithm 2 – employing a null-space filter
- algorithm 3 – includes additional full rank mapping

3. ALGORITHMS REMOVING THE NULL-SPACE INSTABILITY

3.1. Algorithms 1 – improving the gradient of the shape function

In case $N_p \gg N_n$, the rank of the matrix $\nabla\mathbf{N}$ is restricted by the number of nodes (rank($\nabla\mathbf{N}$) $\leq N_n$). Therefore, null($\nabla\mathbf{N}$) > 0 and the null-space stability condition can only be satisfied if null($\nabla\mathbf{N}^{\mathbf{T}}$) $= 0$. The rank(∇N) depends on both the material point discretization and the choice of the gradient of the shape function. Therefore, to satisfy the null-space stability condition, we can select higher order shape function, leading to higher order gradient of the shape function ∇N such that rank(∇N) $= N_n$. Then it satisfies the null-space stability condition as null($\nabla\mathbf{N}^{\mathbf{T}}$) $= 0$.

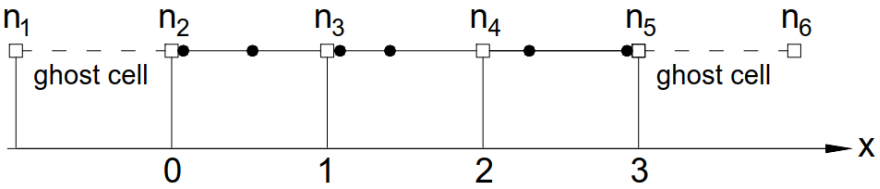

Figure 2. Irregular material point generation

To further examine the influence of the gradient of the shape function in the null-space stability condition, we compute the null-space for different types of gradient of the shape function (MPM, GIMP, DDMP and cubic B-splines) in a one-dimensional example. The domain consists of 6 material points generated irregularly, with 2 material points per cell. The grid has four main nodes ($N_n^{main} = 4$). Figure 2 presents the geometry, where the material points position is indicated by the black dots and nodes are shown as empty squares. The Generalised Interpolation Material Point Method requires additional ghost cells for the mapping (extra nodes). Consequently, the linear mapping extends its dimensions thanks to the ghost nodes. In this example, the number of ghost nodes is equal to two ($N_n^{ghost} = 2$). Therefore, the

total nodes for the GIMP are: $N_n = N_n^{main} + N_n^{ghost} = 4 + 2 = 6$

Table 1. Null-space computations for different computations

Choice of $\nabla\mathbf{N}$	$\boldsymbol{N_p}$	$\boldsymbol{N_n}$	rank($\nabla\mathbf{N}$)	null($\nabla\mathbf{N}$)	null($\nabla\mathbf{N}^{\mathbf{T}}$)
MPM	6	4	3	3	1
GIMP	6	6	5	1	1
DDMP	6	4	3	3	1
Cubic B-splines	6	4	4	2	0

Table 1 shows results of the null-space computation of the problem in Figure 2, based on equation (5). The results shown are for the linear mapping $\nabla\mathbf{N}^{\mathbf{T}}$ as in the four different formulations of the material point method. Based on the null-space stability condition, the linear mappings of the MPM, GIMP and DDMP were considered as unstable because they can generate the null-space leading to errors. In contrast, B-splines MPM in the shown example is a stable formulation because it satisfies the null-space stability condition.

To additionally demonstrate the null-space errors, we simulate a one-dimensional propagation of a compression wave. A compression wave is generated in the middle of an elastic bar with Young's modulus E = 0.04Pa and a length L = 4m. The initial strain is:

$$\varepsilon^o(x, t = 0) = -0.12e^{-60(x-L/2)^2} \tag{6}$$

The analytical solution for that problem at time t is:

$$\varepsilon^t(x, t) = 0.0005\left(e^{-60\left((x-L/2)-0.01t\right)^2} + e^{-60\left((x-L/2)+0.01t\right)^2}\right) \tag{7}$$

In the numerical model, the bar is discretized regularly with 2 material points per cell on a grid made from 400 cells. The problem aim is to investigate only the null-space noise. Therefore, the solution employs small amplitude of strain which means that no single material point crosses to a new cell. The gradient of the shape function for node "i" and the corresponding numerical simulations for the MPM, GIMP, DDMP and B-splines, compared with the analytical results are shown in Figure 3 - Figure 10. These results show that the MPM, GIMP and DDMP produce unstable solutions after 500 time steps corresponding to the final time t = 5s. In contrast, the solution obtained using B-splines is stable replicating closely the analytical one. These numerical observations confirm the analyses based on the null-space stability condition. It is interesting to note that both DDMP and B-splines provide a second-order gradient of the shape function but the DDMP shows a significant null-space errors while the B-splines MPM does not. The null-space errors in the DDMP is inherited from the classical MPM because DDMP uses a weight function to averaging the value in MPM ($\nabla\mathbf{N}$(MPM)) and node-based function ($\nabla\tilde{\mathbf{N}}$).

In summary, the analysis shows that the null-space errors affect simulation results significantly. Removing the null-space errors – as shown with the B-splines MPM, leads to much better match of the simulation results with the analytical solution.

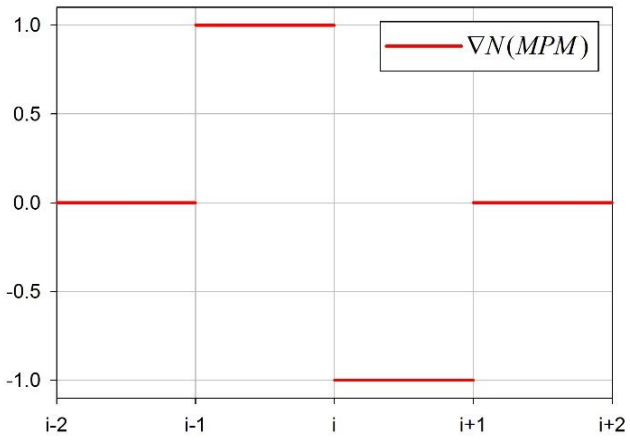

Figure 3. linear-basis gradient of the shape function

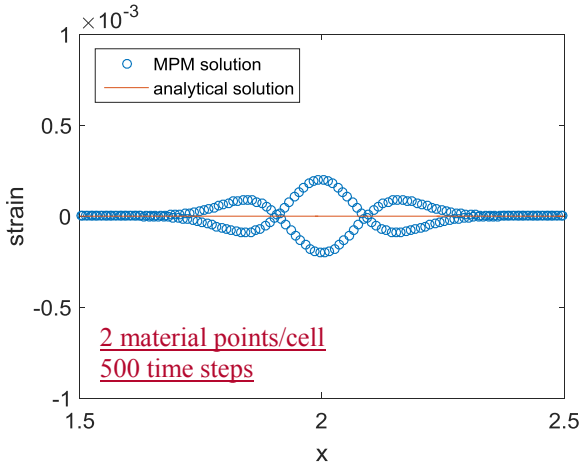

Figure 4. MPM numerical solution

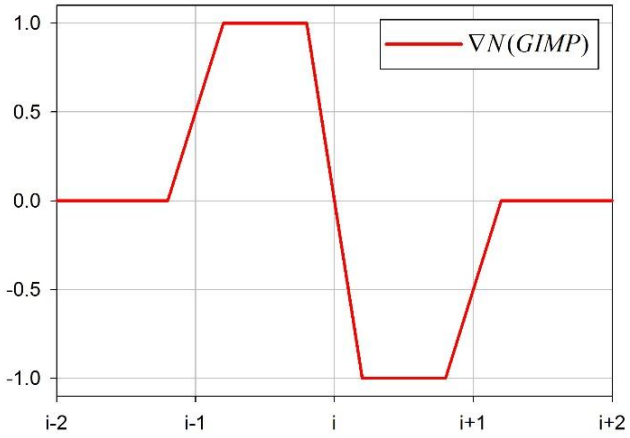

Figure 5. GIMP gradient of the shape function

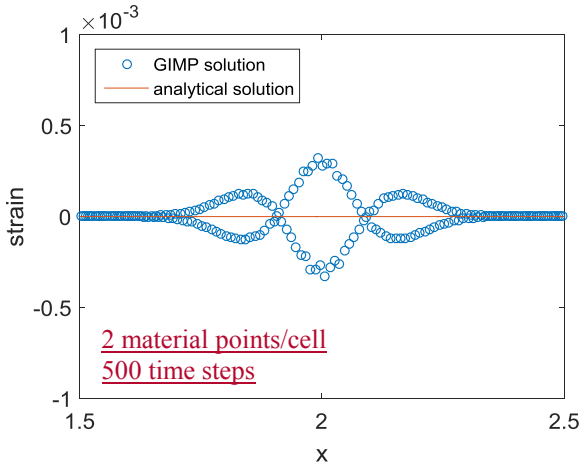

Figure 6. GIMP numerical solution

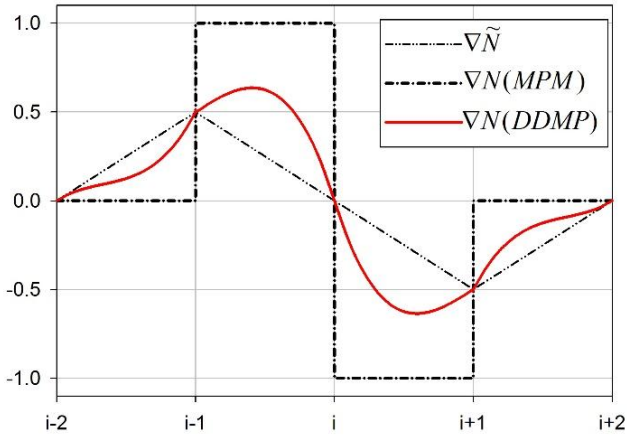

Figure 7. DDMP gradient of the shape function

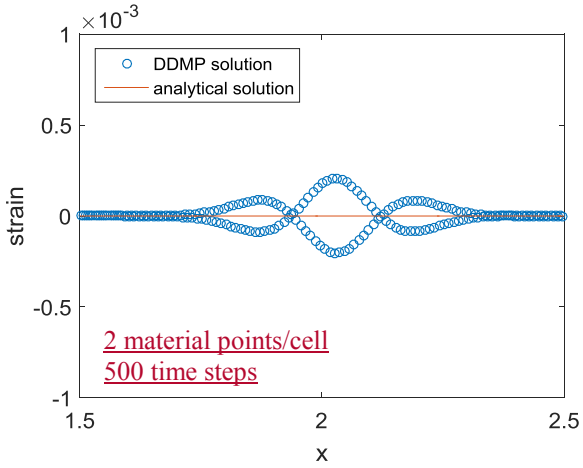

Figure 8. DDMP numerical solution

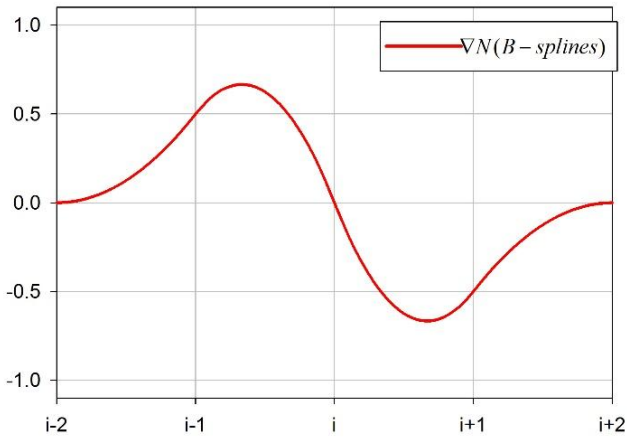

Figure 9. Cubic B-splines gradient of the shape function

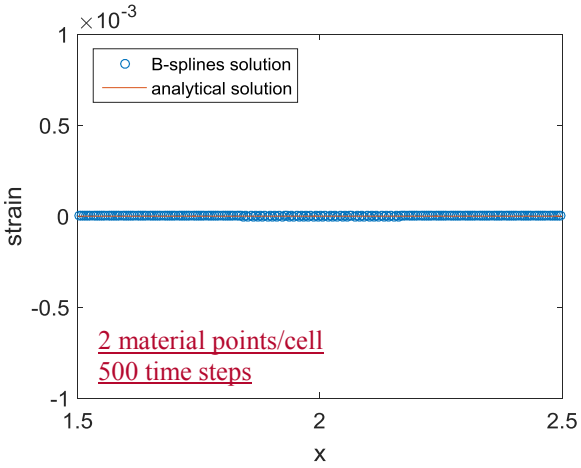

Figure 10. Cubic B-splines numerical solution

3.2. Algorithm 2 – null-space filter

When the MPM solution does not satisfy the null-space stability condition, the algorithm can be enhanced so it would remove the null-space errors in other way, i.e. $\nabla \mathbf{v_p^{null}}$. In this case, instead of satisfying the null-space stability condition as in the case above, we remove the null-space components (errors) in the solutions at every time step (see Figure 11). Therefore, the non-null-space solution at the next time step "k+1" could be calculated as:

$$\nabla \mathbf{v_p^*} = \nabla \mathbf{v_p} - \nabla \mathbf{v_p^{null}} \tag{8}$$

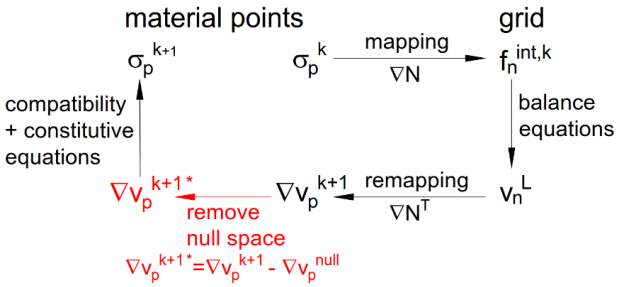

Figure 11. Schematic of solution 2 – null-space filter

In the classical MPM, the matrix $\nabla \mathbf{N}$ has a non-trivial null-space. Gritton and Berzin [12] proposed a SVD method to remove the null-space. Similarly, this paper adopts the QR method using Householder Triangularization algorithm [13] which is less numerically expensive than the SVD computation for both global and local filter. In the MPM formulation, the matrix $\nabla \mathbf{N}^{\mathrm{T}}$ can be written in the reduced QR factorization form as follows:

$$\nabla \mathbf{N}^{\mathrm{T}}{}_{\mathrm{N_p\ x\ N_n}} = \mathbf{Q}_{\mathrm{N_p\ x\ N_n}} \cdot \mathbf{R}_{\mathrm{N_n\ x\ N_n}} \tag{9}$$

where $\mathbf{Q}$ is the unitary matrix which the columns $\boldsymbol{q}_i$ $(i = [1\ N_n])$ are orthonormal and span in the space $\mathbb{R}^{N_n}$. Considering an arbitrary vector $\nabla \mathbf{v_p}$, the null-space component ($\nabla \mathbf{v_p^{null}}$) of the

vector $\nabla \mathbf{v_p}$ is orthogonal to the orthonormal set $\{\boldsymbol{q}_1, \boldsymbol{q}_2, \dots, \boldsymbol{q}_r\}$ with $r = rank(\nabla \mathbf{N}) = rank(\mathbf{R})$. Therefore, the non-null-space solutions ($\nabla \mathbf{v_p^*}$) are the projections of the vector $\nabla \mathbf{v_p}$ in the subspace $\mathrm{Q} = \mathrm{span}(\mathbf{q}_i)$ with $\{\boldsymbol{q}_1, \boldsymbol{q}_2, \dots, \boldsymbol{q}_r\}$.

$$\nabla \mathbf{v_p^*} = \mathrm{Proj_Q}(\nabla \mathbf{v_p}) = \sum_{i=1}^{r} (\boldsymbol{q}_i^T \nabla \mathbf{v_p}) \boldsymbol{q}_i \tag{10}$$

In MPM, $r = rank(\nabla \mathbf{N}) = N_c$ with N_c is the number of cells. Although equation (9) is written in a global form, in practice, we apply the null space filter locally, for each grid cell. Therefore, the size of the matrix $\nabla \mathbf{N}_{local}$ is $N_{pc}\, x\, N_{nc}$ with $rank(\nabla \mathbf{N}_{local}) = 1$ (N_{nc} is the number of nodes of the cell and N_{pc} is the number of material points inside the cell). Application of the local filter is significantly less expensive numerically than the global filter. Figure 12 shows the numerical solutions for the DDMP with null-space filter, using QR method. The results show that the local QR method can remove the null-space errors in the solutions at lower computational cost than the local SVD method. Figure 13 compares the computation costs for the given example in the section 3.1. The difference of computation costs between the SVD method and QR method will be larger when bigger, multi-dimensional problems are considered. The difference will also increase in line with the number of calculated time steps.

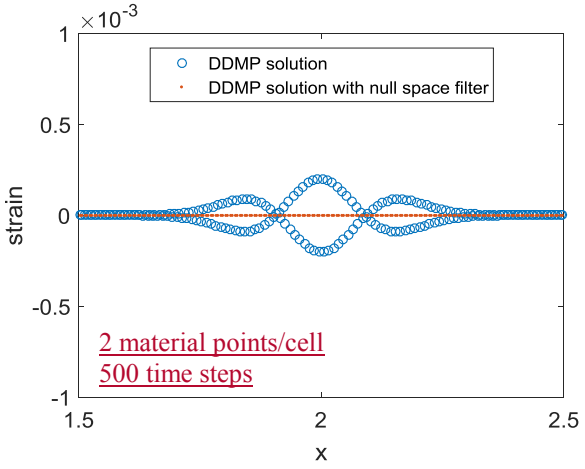

Figure 12. Numerical solution in DDMP with and without null-space filter

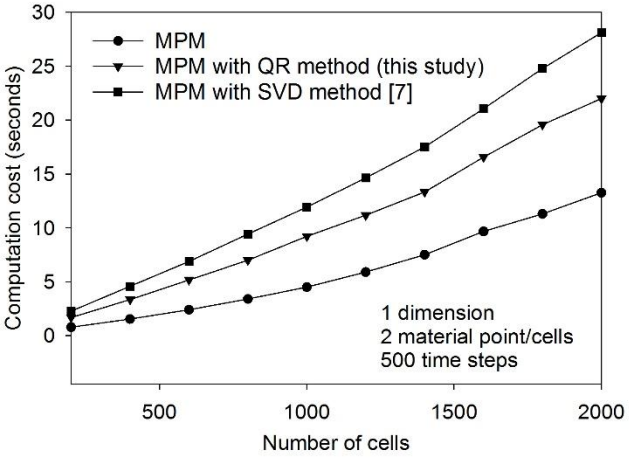

Figure 13. Computation costs of the null-space filter

3.3. Algorithm 3 – additional full rank mapping

Finally, if the mapping in the MPM does not satisfy the null-space stability condition, at the end of each time step, we can apply an additional full-rank mapping to remove the null-space. For example, in MPM, the shape function mapping ($\mathbf{N}$) can be used because the shape function mapping is full rank ($\mathrm{rank}(\mathbf{N}) = \min(N_p, N_n)$). Similar solutions are applied in the literature to improve stress visualization [14] or local null-space filter [12] (see Figure 14). However, an additional mapping can cumulate additional errors through the mapping. Therefore, we do not present this solution in greater detail.

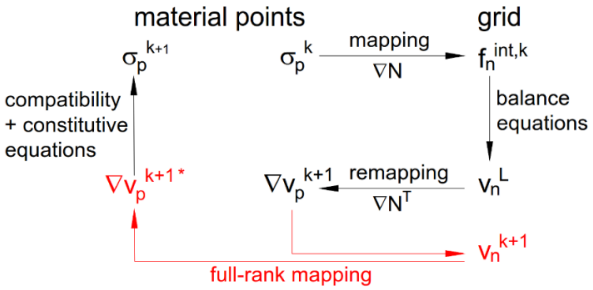

Figure 14. Schematic of solution 3

4. APPLICATION TO THE HYDRO-MECHANICAL PROBLEMS

In this section, we show the application of null-space filter to the hydro-mechanically coupled problem. The hydro-mechanically coupled balance equations base on the velocity-velocity formulation [15] The momentum balance equations for the liquid and solid phase are:

$$n\rho_w \boldsymbol{a_w} = -n\nabla p_w + n\rho_w \boldsymbol{b_w} - \boldsymbol{f_d} \tag{11}$$

$$(1-n)\rho_s \boldsymbol{a_s} = \nabla.\sigma' - (1-n)\nabla p_w + (1-n)\rho_s \boldsymbol{b_s} + \boldsymbol{f_d} \tag{12}$$

where n is the porosity, ρ_w is the liquid density, $\boldsymbol{a_w}$ is the liquid accelerations, $\boldsymbol{b_w}$ is the liquid body force, $\boldsymbol{f_d}$ is the dragging momentum determined from the Darcy law. For the solid phase, $\mathbf{a_s}$ is the solid accelerations, ρ_s is the solid density, $\mathbf{b_s}$ is the solid body force. The hydro-mechanical formulation was first implemented in MPM [16]. Later, it was extended to GIMP [17] and to DDMP [8] as those methods mitigate the cell-crossing errors. These formulations were validated for the small strain problems. In the small strain regime, usually the null-space errors in the pore water pressure profile are small in the hydro-coupled simulations. However, the null-space errors are cumulated significantly quicker in large deformation problems. In this paper, the algorithm 2 – additional null space filter with QR method was used to remove the null-space component of volumetric liquid strain in the solution. That led to a stable pore water pressure also in the large strain regime.

To demonstrate the null-space filter in the hydro-mechanically coupled DDMP formulation, we simulate two examples including gravity loading and consolidation. The problem is one dimensional, where 1m high elastic column of fully saturated porous material is discretized in 100 soil material points and 100 water material points. The grid cell size is l_p = 0.02m leading to 50 cells with 2 material points per cell. Young's modulus of the soil is 10 MPa, the density

$\rho_s = 2143$ kg/m^3, the initial porosity $n_o = 0.3$ and the initial permeability $k_o = 10^{-3}$ m/s. The bulk modulus of the water is 2200 MPa with the water density $\rho_w = 1000$ kg/m^3. The time step is 10^{-6} which satisfies the Courant condition. To generate the null-space errors, we select in case (i) high value of gravity (alternatively the solution could be obtained with a low Young's modulus) and in case (ii) high consolidating pressure. The obtained solutions of hydro-mechanically coupled DDMP with and without null-space filter are compared.

Figure 15 presents the large strain gravity loading simulations with the gravitational acceleration g = 1500 m/s. The saturated soil column reached equilibrium condition after 2 seconds, corresponding to 2 million time steps. Upon examination of Figure 15, it is evident that the accuracy of the pore water pressure using the null-space QR filter in the equilibrium condition is greatly improved and only minimal deviation from the analytical solution can be seen. For the large strain consolidation simulations, the consolidating pressure was equal to 2 MPa. The numerical solution was compared with the large strain consolidation analytical solution [18] at the degree of consolidation (U_s) of 0.05 and 0.5 respectively (see Figure 16 and Figure 17). The mismatch at the beginning of consolidation (U_s =0.05) is due to the reflection from the boundary. Nevertheless, the consolidation simulations show a significant null-space errors accumulating with time while those errors were removed by using the QR method leading to accurate long-term solution.

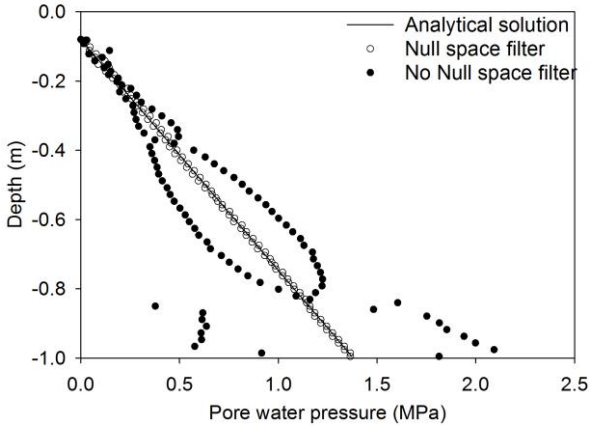

Figure 15. Large strain gravity loading using DDMP with null-space filter

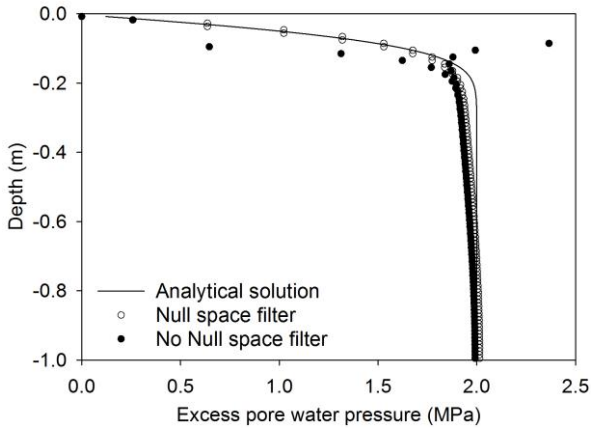

Figure 16. Large strain consolidation using DDMP with null-space filter, $U_s = 0.05$

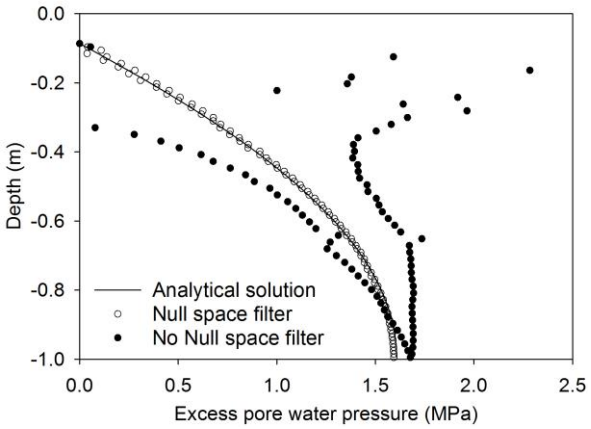

Figure 17. Large strain consolidation using DDMP with null-space filter, $U_s = 0.5$

5. CONCLUSION

This paper investigates null-space errors in the MPM formulations. First, a null-space stability condition is established to examine the null-space errors. If the mapping in the MPM is full rank, the formulation becomes stable. In contrast, the formulation is unstable if the mapping is rank deficient. Furthermore, the null-space stability condition was used to analyse different MPM formulations. The results show that while the classical MPM, GIMP and DDMP contain a rank deficient mapping, the cubic B-splines MPM have a full rank mapping and therefore, B-splines MPM formulation can reduce the null-space errors.

Alternative solutions are introduced such as a null-space filter formulation. As a novelty, we propose QR method to remove entirely null-space errors. The proposed method is similar to the SVD method [12] but requires significantly less computations. Finally, the QR method is used to the hydro-mechanical large strain simulations. The results show that the QR method can reduce greatly the noise due to null-space errors. Currently, we are working to scale up the method for multi-dimensional models and investigate the computational cost more closely.

Acknowledgement: This research was funded by the Academy of Finland under the project 'Progressive failure and post-failure modelling of slopes with Generalized Interpolation Material Point Method (GIMP)' under decision number 286628.

REFERENCES

[1] J. U. Brackbill. The Ringing Instability in Particle-in-cell calculations of low-speed flow. *Journal of computational physics* (1988) **75**:469-492.

[2] E. Edwards y R. Bridson. A high-order accurate particle-in-cell method. *International Journal for numerical methods in engineering* (2012) **90**(9):1073-1088.

[3] C. Gritton, M. Berzins and R. Kirby. Improving accuracy in particle methods using null spaces and filters. *In: Onate E, Bischoff M, Owen DRJ, Wriggers P, Zohdi T (eds) Proceedings of the IV International Conference on Particle-based Methods*, Barcelona, Spain, 2015.

[4] C. C. Hammerquist and J. A. Nairn. A new method for material point method particle updates that reduces noise and enhances stability. *Computer methods in applied mechanics and engineering* (2017) **318**:724-738.

[5] D. Sulsky, S. J. Zhou and H. L. Schreyer. Application of a particle-in-cell method to solid mechanics. *Computer Physics Communications* (1995) **87**:236-252.

[6] S. Badenhagen and E. Kober. The generalized interpolation material point method. *Computer Modeling in Engineering & Science* (2004) **5**:477-495.

[7] L. T. Tran, J. Kim and M. Berzin. Solving time-dependent PDEs using the material point method. *International journal for numerical methods in fluids* (2010) **62**:709-732.

[8] Q. A. Tran and W. Solowski. Large strain consolidation modelling using Dual Domain Material Point Method. *The 15th International Conference of the International Association for Computer Methods and Advances in Geomechanics*, Wuhan, China, 2017.

[9] W. Solowski and S. Sloan. Evaluation of material point method for use in geotechnics. *International Journal for Numerical and Analytical methods in Geomechanics* (2015) **39**:685-701.

[10] M. Steffen, R. M. Kirby and M. Berzins. Analysis and reduction of quadrature errors in the material point method. *International Journal for numerical methods in engineering* (2008) **76**:922-948.

[11] D. Zhang, X. Ma and P. Giguere. Material Point Method enhanced by modified gradienet of shape function. *Journal of Computational Physics* (2011) **230**:6379-6398.

[12] C. Gritton and M. Berzins. Improving accuracy in the MPM method using a null space filter. *Computational Particle Mechanics* (2016) **3**:1-12.

[13] L. N. Trefethen y L. David Bau. *Numerical Linear Algebra*. SIAM, 1997.

[14] S. M. Andersen and L. V. Andersen. Analysis of Stress Updates in the Material Point Method. *In L. Damkilde, L. Andersen, A. S. Kristensen, & E. Lund (Eds.), The Nordic Seminar on Computational Mechanics* (2009):129-134.

[15] O. C. Zienkiewicz and T. Shiomi. Dynamic behaviour of saturated porous media: the generalized Biot formulation and its numerical solution. *International Journal of Numerical and Analytical Methods in Geomechanics* (1984) **8**(1):71-96.

[16] S. Bandara and K. Soga. Coupling of soil deformation and pore fluid flow using material point method. *Computers and Geotechnics* (2015) 63:199-214.

[17] C. Liu, Q. Sun, F. Jin and G. G. D. Zhou. A fully coupled hydro-mechanical material point method for saturated dense granular materials. *Powder Technology,* in Press, 2017.

[18] K. H. Xie and C. J. Leo. Analytical solutions of one-dimensional large strain consolidation of saturated and homogeneous clays. *Computers and Geotechnics* (2004) **31**:301-314.

[19] D. Sulsky and M. Gong. Improving the Material Point Method. *Innovative Numerical Approaches for Multi-Field and Multi-Scale Problems. Lecture notes in Applied and Computational Mechanics* (2016) **81**:217-240.